Swansea University
Prifysgol Abertawe

Cronfa
Setting Research Free

Cronfa - Swansea University Open Access Repository

_____

This is an author produced version of a paper published in :
Desalination

_____

Cronfa URL for this paper:
http://cronfa.swan.ac.uk/Record/cronfa27773

_____

Paper:

_____

Microfiltration of micro-sized suspensions of boron-selective resin with PVDF membranes

Nawaf Bin Darwish[a], Victor Kochkodan[b], Nidal Hilal*[c]

a National Center for Water Treatment and Desalination Technology, King Abdul Aziz City for Science and Technology (KACST), Riyadh, Saudi Arabia

b Qatar Environment and Energy Research Institute (QEERI), Hamad bin Khalifa University (HBKU), Qatar Foundation, Doha, Qatar

c Centre for Water Advanced Technologies and Environmental Research (CWATER), College of Engineering, Swansea University, Swansea SA2 8PP, United Kingdom

Highlights

- Microfiltration of Amberlite IRA743 resin suspensions was studied.
- Formation of a cake layer is a dominant fouling mechanism.
- The flux increases with the feed pH, while declines with operating pressure.
- The resins can be efficiently concentrated by microfiltration and reused.
- Membrane fouling during microfiltration should be further addressed.

Abstract

In this paper microfiltration (MF) separation of fractionized ion exchange Amberlite IRA743 resin from aqueous solutions using polyvinylidene fluoride membranes with the pore sizes of 0.1, 0.22 and 0.45 μm was studies. The effect of membrane pore size, transmembrane pressure, pH and concentration of the resin suspensions, presence of NaCl, MgCl2 and Na$_2$SO4 salts on permeate flux has been evaluated. It was shown that the dominant membrane fouling mechanism during MF of the resin suspensions is formation of a cake layer from deposited resin on the membrane surface. The flux declines with increasing operating pressure and suspension concentration, while it increases with the presence of inorganic salts and feed pH. Changes in zeta potential of resin particles and the membranes as well as agglomeration and electroviscous effects should be considered while analyzing these findings. It was shown that the resin particles after boron sorption can be efficiently regenerated and reused in combined adsorption-microfiltration (AMF) process of boron removal from water, however a sharp drop in membrane flux during MF separation of the resin suspension should be further addressed to develop the efficient AMF procedure.

Keywords: Microfiltration; PVDF membranes; Amberlite IRA743 resin; Boron removal

*Corresponding author: n.hilal@swansea.ac.uk

1. Introduction

During the recent years, increased attention has been given to boron removal from water[1] and [2]. Although boron content in water at concentration of 0.3 mg/L or less, is beneficial for both humans' consumption and irrigation, however, at higher boron levels it can be hazardous to humans, plants and animals [3] and [4]. Accordingly to current World Health Organization guidelines on drinking water quality, the recommended boron content in drinking water is established as 2.4 mg/L [5]. It should be noted the existing guidelines are still provisional values that are subject to further discovery of boron toxicity on human beings.

In the Middle East and North Africa region a large amount of drinking water and irrigation water is produced by reverse osmosis (RO) desalination of seawater [6]. However boron removal with RO membranes are often insufficient under common RO conditions[7] and [8]. Therefore, there is a strong need both for upgrading the efficiency of conventional boron treatment processes [9] and [10] and searching for novel approaches for boron removal from water such as, for example, a combined adsorption-microfiltration (AMF) process [11], [12] and [13]. In this process, boron is first sorbed by boron selective resins, which are then separated from feed by microfiltration (MF). Kabay et al. investigated the AMF efficiency for boron removal from model boron-containing solutions[11] and [12], seawater [13], [14] and [15] and geothermal water [16]. It was reported that AMF process can be considered as an alternative for polishing treatment of RO permeate [17]. The main benefit of the hybrid AMF process of boron removal from water over conventional fixed-bed ion-exchange treatment is the higher efficiency. In the combined AMF system the fine resin particles with high surface area may be used to improve the sorption rate [17]. This reduces the amount of the sorbent required and decreases the operating costs of the water deboronization. It was also reported [18],[19] and [20] that the consumption of chemicals and energy with AMF are much lower compare to fixed-bed ion exchange treatment.

Although numerous papers have been published on the AMF process [11], [12], [13],[14], [15], [16], [17], [18] and [19] they focused mainly at efficiency of boron removal with the boron-selective resins from different feeds, however the studies on how membrane pore size, pH and ionic strength of the feed affect the membrane flux and separation of boron-saturated resins are still rare [20] and [21]. Ondercova et al. [20] and Blahusiak at al. [21] used the tubular ceramic membranes of 0.1 μm pore size to simulate and concentrate suspensions of Dowex XUS resin with the mean particle size of 4.7 μm at suspension concentrations of 0.0015 to 20 wt.%, and different crossflow velocities and operating pressures. However the effect of pH and ionic strength of the feed on MF separation of the resin suspension as well as the analysis of surface morphology of the membranes before and after filtration have been not considered. In our previous work boron sorption from salty solutions with fractionized Amberlite IRA743 resin particles over a wide boron concentration range was investigated [22]. The purpose of this study to investigate the

effect of membrane pore size, transmembrane pressure, pH, ionic strength on separation of boron-saturated fractionized Amberlite IRA743 particles with MF polyvinylidene fluoride (PVDF) membranes of different pore size of 0.1, 0.22 and 0.45 μm. Special attention is also given to the evaluation of the possibility of multiple using of MF concentrated suspensions of Amberlite IRA743 resin by performing of three consecutive sorption-elution-reconditioning cycles. The membranes' surface morphology before and after the concentration of the resin suspensions is also studied to provide addition information regarding membrane fouling issues. The insight into this phenomenon is important for choosing an optimal membrane and feed composition to develop an efficient AMF process for boron removal from water.

2. Experimental

Amberlite IRA743 resin was supplied from Sigma-Aldrich (UK); boric acid (99.5%) was purchased from Fisher Scientific (UK). The initial resin with particle size of 500–700 μm was ground using a ball mill and sieved by 45 μm sieve to get the fractionized resin particles. As seen in Fig. 1, the resin particle size was ranging from 1 to 110 μm with the peak observed at 45 μm. The BET surface area of the Amberlite IRA743 resin particles was found as 26.6 m^2/g.

A combined AMF system was designed and built to investigate the effect of operating parameters on boron removal and MF of the resin suspensions. A flow sheet of AMF process is shown in Fig. 2. Feed solution is mixed with boron-selective Amberlite IRA743 resin in tank 1 (T1) to provide the solute removal from water. After boron sorption the resin suspension fed to MF cell (MF1) to separate the boron-saturated resin particles from water. Boron free permeate (permeate 1) can be used as product water while the concentrated suspension of exhausted Amberlite IRA743 resin particles is supplied to tank 2 (T2), where HCl solution is added to elute the boron from the resin. The regenerated resin was further concentrated in MF2 cell and fed to tank 3 (T3), where it was washed with MilliQ water followed by pH adjusting with NaOH solution. Then the regenerated and reconditioned resin was concentrated in MF3 cell and returned to tank 1 for the next boron sorption cycle. The volume of each tank was equals to 7 L. The membrane effective area in the MF cells was 0.00332 m^2 and a height of the feed channel over the membrane surface was 2 mm. The membrane cells were operated in cross-flow mode and a flow velocity was kept at 0.15 m/s. The pipes of the AMF system were made of stainless steel with an inner diameter of 4 mm and an outer diameter of 6 mm.

The flat sheet hydrophilized PVDF membranes (GVWP, Millipore) with pore size 0.1, 0.22 and 0.45 μm were used in the experiments. A fresh piece of membrane was used in all filtration experiments. Prior to the filtration of a feed suspension, MilliQ water was filtered through a membrane at the desired operating pressure for 15 min.

Boron concentrations in feed solutions were chosen as 5.0 and 1.5 mg/L to represent average boron content in seawater and in permeate from a first RO seawater desalination stage, respectively. Boric acid solutions were prepared by dissolving the appropriate amount of boric acid in distilled water. A pH value of the solution was adjusted with 0.2 N HCl or 0.2 N NaOH. Concentration of boron was determined with Hach DR-2400 pectrophotometer by Carmine method.

The efficiency of boron removal (R) from water was calculated using the following equation:

$$R = \frac{C_0 - C_e}{C_0} \times 100$$

Equation 1

where C_0 and C_e are the initial and equilibrium boron concentration (mg/L), respectively. The operating pressure used was varied from 0.2 to 1.5 bar while the concentration of Amberlite IRA743 resin suspensions was changed from 0.2 to 1 g resin/L. The content of NaCl, MgCl2 and Na2SO4 salts in the feed were chosen in the range of their concentration in seawater.

A Malvern Mastersizer-2000 analyzer was used to evaluate the particle size distribution of the Amberlite IRA743 resin by measuring the intensity of light scattered as a laser beam passes through a dispersed particulate sample.

Zeta potentials of the membranes were determined using an electrokinetic analyzer, EKA (Anton Paar KG, Austria). The zeta potentials of resin particles were determined using a Malvern Zetasizer 300HSA instrument.

The surface and cross-section membrane images were taken by scanning electron microscope (SEM) Hitachi S-4800II (Japan). The polymeric membrane sample was frozen rapidly, and then fractured by simply breaking or by using tweezers while maintained at liquid nitrogen temperature. The sample was mounted onto a stub, then coated with approximately 10 nm of gold to make it conductive and finally the sample stub was inserted to the SEM chamber in high vacuum mode to take an image.

3. Results and discussion

As known molecules of boric acid $B(OH)_3$ dissociate in aqueous solution to form tetrahydroxyborate ions $B(OH)_4^-$ as confirmed by Raman spectroscopy [18]:

The *pK* values of boric acid have been determined to be *pKa* = 8.60 in artificial seawater at temperature of 25 °C and salinity of 35 g/L [23] and pK_a = 9.24 at 25 °C in fresh waters[24]. When Amberlite IRA 743 resin is used for boron removal, the borate ion is complexed with hydroxyl groups of *N*-methyl-D-glucamine groups to form bidentate complex [25]. To provide multiple AMF cycles for water treatment the boron-saturated resin particles should be separated from feed, regenerated and used repeatedly. In this work MF separation of boron-saturated fractionized resin particles from treated water with PVDF membranes of 0.1–0.45 μm pore size was studied at various operational conditions and feed composition.

3.1. Effect of membrane pore size on permeate flux

It was found that the pure water fluxes through the membranes conforms to Darcy's law and are directly proportional to the applied pressure. At operating pressure of 1 bar the fluxes are 3325, 7581 and 26,439 L/m^2 × h for PVDF membranes of pore size of 0.1, 0.22 and 0.45 μm, respectively.

Fig. 3 and Fig. 4 present data on permeate flux during MF of the resin suspension at different operating pressures.

As seen in these Figures for constant operating pressure the flux increased when PVDF membrane pore size changed from 0.1 μm to 0.22 μm but a flux decline was found when 0.45 μm MF membrane was used. Pseudo-steady fluxes were 275, 389, and 358 L/m^2 × h at operating pressure of 0.5 bar and 401, 655, and 600 L/m^2 × h at 1.5 bar for PVDF membranes of 0.1, 0.22 and 0.45 μm pore size, respectively.

The variation of membrane flux with filtration time can be divided into two regions, a quickly decay and a pseudo-steady stage (Fig. 3 and Fig. 4). At the beginning of the process the filtration rate is determined by the transmembrane pressure and by the intrinsic membrane resistance. The filtrate flow causes convective particle transport to the membrane and the membrane flux attenuates very quickly due to the resin particles deposition on the membrane surface and formation of a cake layer [25] and [26]. Because of this layer grows on the membrane surface the cake resistance increases and the flux declines with filtration time. The flux decrease becomes very slow after about 400 s of filtration time. It should be noted that a lower pseudo-steady filtration flux was found for the membrane with the larger pore size of 0.45 μm compare to 0.22 μm PVDF membrane. Though the used resin particles are larger than the average membrane pore size, obviously because of the pore size distribution some smaller particles, nevertheless might penetrate in the porous structure of the membrane. This phenomenon becomes less obvious under a lower filtration pressure [25]. It should be noted that permeate was analyzed to check a content of total dissolved solids and it was found that the resin particles were completely rejected on the membranes.

As filtration proceeds the cake layer increases in mass and thickness, the permeate flux decreases to an extent which is determined by the hydraulic properties of the deposited layer of the resin particles.

A degree of membrane fouling during MF of the suspension of the resin particles was calculated quantitatively based on the Darcy law and a resistance in series model[27] and [28]. According to this model the membrane flux can be described as

$$J = \Delta P/(\eta \cdot R_t)$$

where J is permeation flux (ms^{-1}), ΔP is transmembrane pressure difference (Pa), R_t is total filtration resistance (m^{-1}), and η is viscosity of solution (Pas).

It is assumed that total filtration resistance (R_t) is the sum of intrinsic membrane resistance (R_m), fouling resistance caused by internal pore fouling with particles (R_i) and resistance of the cake layer formed on membrane surface with deposited resin particles (R_c): $R_t = R_m + R_i + R_c$. Those resistances can be calculated from experimental data using the following equations:

$$R_m = \frac{\Delta P}{\eta J_{w1}}$$

$$R_i = \frac{\Delta P}{\eta J_{w2}} - R_m$$

$$R_c = \frac{\Delta P}{\mu J_s} - R_m - R_i$$

where J_s is the flux during MF of the resin suspension at quasi steady state, J_{w1} the initial water flux and J_{w2} the final water flux after removing a cake layer. The cake layer was removed from the membrane surface by a sponge.

The membrane resistances and their relative percentages for different PVDF membranes during MF of the resin suspension are presented in Fig. 5. As seen in this Figure the intrinsic membrane resistance R_m remains low and doesn't exceed 4% of the total hydraulic resistance R_t. The internal fouling resistance R_i slightly increased from 2% to 7% for PVDF membranes with pore size of 0.1 and 0.45 μm respectively, obviously because of penetration of the smallest resin particles in the porous structure of the membrane. The cake layer formed by resin particles on the membrane surface during MF of the resin suspensions represent the major fouling resistance R_c, which is 91–94% of the total filtration resistance R_t.

3.2. Effect of transmembrane pressure on permeate flux

The change in permeate flux with filtration time for PVDF membranes with different pore sizes at different operating pressures is shown in Fig. 6, Fig. 7 and Fig. 8.

As seen in Fig. 6, Fig. 7 and Fig. 8, at higher operating pressure the initial membrane flux is larger however it declines more rapidly with filtration time. Fig. 6 shows that after filtration for 5 min the permeate flux declines by 44% and 16% at transmembrane pressure of 1.5 and 0.2 bar, respectively. This behavior shown can be explained by faster particle accumulation in the cake layer on the membrane surface at higher operating pressure [29]. Rapid flux decline at high operating pressure may also be attributed to the formation of a more densely packed cake layer from deposited resin particles on the membrane surface. It has been experimentally shown that cake layers can be more compressed at high operating pressures due to a drag force induced by permeate flow[30].

As filtration time progresses toward pseudo-steady state, the difference between the permeate fluxes at the applied pressures decreases. Fig. 7 shows that the difference between the permeate fluxes at the beginning and the end of filtration cycle decrease from 62% to 19% at operating pressures of 1.5 and 0.2 bar. At this stage of the filtration process, the flux behavior is controlled to a large extent by the resistance of the cake layer. Since thicker, and thus more resistant, cake layers are formed at higher applied pressures, the effect of the increased pressure on the permeate flux is not as significant at the latter stages of the filtration [29].

As seen in Table 1 the intrinsic membrane resistance Rm is negligible during MF of the fractionized resin suspension and does not practically vary with operating pressure, whileRi and especially Rc resistances increase with operating pressure, that results in a higher value of total filtration resistance Rt.

3.3. Effect of the suspension concentration on the permeate flux

As seen in Fig. 9, the permeate flux for 0.1 μm PVDF membrane decreased with an increase of the suspension concentration. The initial fluxes are 761, 672, 597, and 258 L/m^2 × h, while the pseudo-state permeate fluxes are 420, 350, 250 and 190 L/m^2 × h at the resin dosage of 0.2, 0.4, 0.6 and 1.0 g/L respectively. The larger permeate flux decline at higher concentration of the resin suspension is attributed to the increased particle transfer rate to the cake layer [29]. According to Hong et al. [30] the growth of the deposited layer is proportional to the convective particle flux entering the cake layer. Thus, an increase in feed particle concentration enhances particle accumulation in the cake layer, which results in increased its hydraulic resistance and in the flux decline [30].

The hydraulic resistances and their relative percentages for 0.1 μm PVDF membrane during MF of the resin suspensions of different concentration are presented in Fig. 10. As seen in this Figure both the intrinsic membrane resistance Rm and the internal fouling resistance Ri remains low and doesn't change notably with an increase of the resin concentration. However the resistance of the cake layer Rc formed by the resin particles on

the membrane surface essentially increase with the feed suspension concentration and this resistance represent the major membrane fouling resistance.

In addition, there has been some experimental evidence showing the formation of a denser cake layer at higher particle concentrations. Chudacek and Fane [31]demonstrated that the specific resistance of a cake layer increased with increasing particle concentration. It was suggested that this behavior may results from the increased pressure that accumulated particles at the top of the cake layer exert on the particles in the bottom of the layer.

3.4. Effect of pH on permeate flux

The effects of feed pH values on permeate flux with 0.22 μm PVDF membrane is shown in Fig. 11. As seen in this Figure the flux increased with changing pH from 4.0 to 8.0. However, the flux decreased at further pH rising from 8.0 to 10.5. Obviously both changes in zeta potential of resin particles and the membrane should be taken into consideration do describe the findings.

As can be seen in Fig. 12, the Amberlite IRA743 resin particles have an isoelectric point (IEP) at pH 7.8 due to presence of the positively charged tertiary amine in *N*-methyl-D-glucamine functional groups of the polymer matrix. The resin particles carried a net positive charge when pH was lower than 7.8, but were negatively charged at pH above 7.8.

The pristine PVDF membrane, initially having a positive ζ value, passes through an IEP at approximately pH 4 and is negatively charged above pH 4. It was suggested that a decrease in the ζ values with increasing pH is caused by the preferential adsorption of hydroxyl groups on the membrane surface at high pH of aqueous solutions [32].

As seen in Fig. 11 permeate flux is higher at feed pH of 8.0, i.e. near the IEP of the resin particles. Probably the resin particles tend to agglomerate when the pH approaches their IEP, which mainly due to attractive Van der Waals forces and hence a more loose cake layer was deposited on the membrane surface [33]. At pH values far away from IEP the resin particles are better dispersed, due to mutually repulsive electrostatic forces, and denser and higher resistance fouling layers are formed on the membrane surface that results in lower fluxes. It should be noted that a decrease of the membrane flux was observed when the feed pH value was changes from 8.0 to 10.5. This was similar to that observed by Bowen and Gosnaga [34] and may be due to electroviscous effect phenomena. It was suggested [35] that if an electrolyte solution is pressed through a capillary with charged surfaces, ions moved away from their preferred position in the electrolyte double layer, associated with the surface. This can be described as an increase in the apparent viscosity of the solution (electroviscous

effect) that lead to an increase in the filtration resistance and in turn to decrease of the permeate flux.

3.5. Effect of ionic strength of the feed on permeate flux

The effect of NaCl, Na2SO4 and MgCl2 salts at concentration of 5000–35,000; 3000–10,000 and 2000–5000 mg/L, respectively, on the permeate flux during MF of the resin suspension is shown in Fig. 13, Fig. 14 and Fig. 15. The salts concentrations were chosen to represent the average salts content in brackish water and seawater.

As seen in Fig. 13, the permeate flux decayed rapidly during the first 10 min of filtration, followed by a gradual decrease to a pseudo-steady value that varied with the ionic strength of NaCl solution. The pseudo-state flux increases from 1290 to 1401 $L/m^2 \times h$ at NaCl concentration of 5000 and 35,000 mg/L, respectively.

The pseudo-state permeate flux increases from 1435 to 1588 $L/m^2 \times h$ when feed Na2SO4 concentration increases from 3000 to 10,000 mg/L, respectively (Fig. 14).

As seen in Fig. 15, the quasi-state permeate flux increases from 1040 to 1400 $L/m^2 \times h$ at feed MgCl2 concentration of 5000 and 20,000 mg/L, respectively.

The presented results indicate that increasing the ionic strength of the feed resulted in higher fluxes during MF of the resin suspensions. Obviously, these findings may be explained by agglomeration of the resin particles in the feed solutions of high ionic strength. Such agglomeration facilitates due to the decrease in the particles zeta potentials caused by the compression of the diffuse electric layer at the resin surface at high ionic strength of the feed suspension. The particles aggregates form a more permeable cake layer on the membrane surface that result in higher permeate flux. For example, as seen in Table 2 the cake layer resistances (Rc) largely decrease when $MgCl_2$ salt is present in the feed. This results in an essentially decrease of the total filtration resistance Rt. Similar data on increase of water flux, when inorganic salts are presented in the feed, have been reported previously for MF of TiO2 suspensions[36] and [37].

3.6. Multiple MF concentration of the resin suspensions in AMF process of boron removal from water

Previously it was shown [20] that boron-saturated Amberlite IRA743 resin particles can be efficiently regenerated using boron elution with HCl followed by the resin reconditioning with NaOH. In this study, three consecutive sorption-elution-reconditioning AFM cycles were performed to evaluate the main peculiarities of MF concentration of the resin

suspensions in the combined AMF process of boron removal from water (for details see Section 2 and Fig. 2). Table 3 shows the change in permeate flux with filtration time during MF separation of the resin particles for multiple boron sorption, elution and reconditioning steps. After boron sorption in AFM cycle 1 the resin suspension was MF concentrated (see flux data for the boron sorption stage in Table 3). Then the concentrated resin particles were regenerated with 0.2 N HCl: 600 mL of HCl solution were added to the concentrated suspension of the boron saturated resin particles and the suspension was circulated for 10 min before MF separation (flux data for the boron elution stage in Table 3). Thereafter the regenerated suspension was washed with MilliQ water, reconditioned with 0.2 N NaOH: 300 mL of NaOH solution were added to the suspension, kept circulated for 10 min following by MF (flux data for the reconditioning stage in Table 3). The reconditioned suspension was repeatedly used for boron sorption in AMF cycle 2. The same sequence of operations was performed for AMF cycle 3.

It is seen in Table 3 the flux decreased by 58%: from 1929 $L/m^2 \times h$ at the beginning to 799 $L/m^2 \times h$ at the end of MF concentrating of the boron saturated resin suspension after boron sorption in AFM cycle 1. The flux reduction for MF concentrating of the boron saturated resin suspension in AMF cycle 2 is 56%: from 1460 to 631 $L/m^2 \times h$, while the flux declined from 891 to 391 $L/m^2 \times h$ in the boron sorption cycle 3. In total for AFM cycles 1–3 the flux decreased by 80%: from 1929 to 391 $L/m^2 \times h$ during MF concentrating of the resin suspension after boron sorption.

Table 3 shows that the flux decreased from 813 $L/m^2 \times h$ at the beginning to 418 $L/m^2 \times h$ at the end of MF treatment of the regenerated resin suspension after boron elution in AMF cycle 1. For boron elution in cycle 2 the flux reduction is from 616 to 330 $L/m^2 \times h$, while the flux declined from 550 to 264 $L/m^2 \times h$ in AMF cycle 3. In total the flux decreased by 68%: from 813 to 264 $L/m^2 \times h$ at MF concentrating of the regenerated resin suspension after boron elution in AMF cycles 1–3.

During MF of the reconditioned resin suspension in AMF cycle 1 the flux decreased by 68% from 1806 $L/m^2 \times h$ at the beginning to 559 $L/m^2 \times h$ at the end of filtration (Table 3). For the reconditioning cycle 2 the flux reduction was 49%: from 876 to 444 $L/m^2 \times h$, while the flux declined by 33% from 617 to 408 $L/m^2 \times h$ in the reconditioning cycle 3. In total the flux decreased by 77%: from 1806 to 408 $L/m^2 \times h$ during MF of the reconditioned resin suspension in AMF cycles 1–3.

The presented data indicate severe flux reduction during multiple MF concentrating of Amberlite IRA743 resin suspensions after boron sorption, elution and reconditioning of the resins in AMF process (Table 3). As seen from SEM images of PVDF membranes (Fig.

16 and Fig. 17), the flux drop during MF of the Amberlite IRA743 resin suspension is explained by deposition of the resin particles and formation of a thick cake layer on the membrane surface. Thus, the prevention of membrane fouling and recovering of the membrane flux need to be further addresses to develop the efficient AMF procedure for water deboronization.

It should be noted that the boron removal efficiency from water for AMF cycles 1–3 did not vary noticeably and was found as 99–96%. The obtained results prove that the fine Amberlite IRA743 resin particles perform very consistently after multiply sorption- elution-reconditioning cycles and might be efficiently reused in AMF process of water deboronization.

4. Conclusions

Experimental results during MF separation of ion-exchange Amberlite IRA743 resin particles with PVDF membranes of different pore size of 0.1, 0.22 and 0.45 have indicated that the membrane flux declines sharply with increasing operating pressure and the suspension concentration, while the flux increases with ionic strength of the feed. The analysis of the flux decline using the resistance in series model has showed that the dominant membrane fouling mechanism is formation of a cake layer from deposited resin particles on the membrane surface.

It was found that a pH value of the feed suspension essentially affects the membrane flux during MF concentration. At pH values far away from IEP of the resin, the particles are better dispersed, and denser and higher resistance fouling layers are formed on the membrane surface that results in lower membrane fluxes.

The flux increases with the presence of NaCl, MgCl2 and Na_2SO4 salts in the feed, obviously due to agglomeration of the resin particles and formation a more permeable cake layer on the membrane surface at high ionic strength of the resin suspensions.

It was shown that the resin particles saturated with boron can be efficiently separated with MF and repeatedly used in AFM process. The boron removal efficiency of the resin after multiply sorption-elution-reconditioning cycles was found as 99–96%; however, the mitigation of the membrane fouling during MF of the resin suspensions should be further addresses to develop the efficient AMF procedure for boron removal from water.

References

[1] N. Kabay, M. Bryak, N. Hilal (Eds.), Boron Separation Processes, Elsevier (2015)

[2] N. Kabay, E. Güler, M. Bryjak, Boron in seawater and methods for its separation - a review
  Desalination, 261 (2010), pp. 212–217

[3] F.S. Kot, Boron in the environment
  N. Kabay, M. Bryak, N. Hilal (Eds.), Boron Separation Processes, Elsevier (2015), pp. 1–34

[4] F.H. Nielsen, Update on human health effects of boron. J. Trace Elem. Med. Biol., 28 (2014), pp. 383–387

[5] WHO. Guidelines for Drinking Water Quality. (fourth ed.) (2011) Zheneva

[6] N. Hilal, G.J. Kim, C. Somerfield, Boron removal from saline water: a comprehensive review.
  Desalination, 273 (2011), pp. 23–35

[7] H. Polat, A. Vengosh, I. Pankratov, M. Polat. A new methodology for removal of boron from water by coal and fly ash. Desalination, 164 (2004), pp. 173–188

[8] E. Guler, N. Kabay, M. Yuksel, N.O. Yigit, M. Kitis, M. Bryjak. Integrated solution for boron removal from seawater using RO process and sorption-membrane filtration hybrid method. J. Membr. Sci., 375 (2011), pp. 249–257

[9] Y.-T. Wei, Y.-M. Zheng, J.P. Chen, Design and fabrication of an innovative and environmental friendly adsorbent for boron removal, Water Res., 45 (2011), pp. 2297–2305

[10] S. Morisada, T. Rin, T. Ogata, Y.-H. Kim, Y. Nakano, Adsorption removal of boron in aqueous solutions by amine-modified tannin gel, Water Res., 45 (2011), pp. 4028–4034

[11] N. Kabay, I. Yılmaz, M. Bryjak, M. Yuksel, Removal of boron from aqueous solutions by ion exchangemembrane hybrid process, Desalination, 198 (2006), pp. 74–81

[12] I. Yilmaz, N. Kabay, M. Bryjak, M. Yuksel, J. Wolska, A. Koltuniewicz, A submerged-ion exchange hybrid process for boron removal, Desalination, 198 (2006), pp. 310–315

[13] N. Kabay, M. Bryjak, S. Schlosser, M. Kitis, S. Avlonitis, Z. Matejka, I. Al-Mutaz, M. Yuksel, Adsorption-membrane filtration (AMF) hybrid process for boron removal from seawater: an overview, Desalination, 223 (2008), pp. 38–48

[14] M. Bryjak, J. Wolska, N. Kabay, Removal of boron from seawater by adsorption-membrane hybrid process: implementation and challenges, Desalination, 223 (2008), pp. 57–62

[15] M. Bryjak, J. Wolska, I. Soroko, N. Kabay, Adsorption-membrane filtration process in boron removal from first stage seawater RO permeate, Desalination, 241 (2009), pp. 127–132

[16] N. Kabay, I. Yilmaz-Ipek, I. Soroko, M. Makowski, O. Kirmizisakal, S. Yag, M. Bryjak, M. Yuksel. Removal of boron from Balcova geothermal water by ion exchangeemicrofiltration hybrid process, Desalination, 241 (2009), pp. 167–173

[17] A. Koltuniewicz, A. Witek, K. Bezak. Efficiency of membrane-sorption integrated processes

[18] B. Onderkova, S. Schlosser, T. Bakalar, M. Bugel, Microfiltration of concentrated suspensions of a microparticulate ion-exchanger through a ceramic membrane, Sep. Sci. Technol., 42 (2007), pp. 3003–3010

[19] M. Blahusiak, S. Schlosser, Simulation of the adsorption-microfiltration process for boron removal from RO permeate, Desalination, 241 (2009), pp. 156–166

[20] B. Onderkova, S. Schlosser, M. Blahusiak, M. Bugel, Microfiltration of suspensions of microparticulate boron adsorbent through a ceramic membrane, Desalination, 241 (2009), pp. 148–155

[21] M. Blahušiak, B. Onderková, Š. Schlosser, J. Annus, Microfiltration of microparticulate boron adsorbent suspensions in submerged hollow fibre and capillary modules, Desalination, 241 (2009), pp. 138–147

[22] N. Bin Darwish, V. Kochkodan, N. Hilal, Boron removal from water with fractionized Amberlite IRA743 resin, Desalination, 370 (2015), pp. 1–6

[23] A.G. Dickson, Thermodynamics of the Dissociation of Boric-Acid in Synthetic Seawater from 273.15-K to 318.15-K, Deep-Sea Res. A Oceanogr. Res. Pap., 37 (1990), pp. 755–766

[24] J.A. Dean, Lange's Handbook of Chemistry, McGraw-Hill, New York (1999)

[25] C. Jacob, Seawater desalination: boron removal by ion exchange technology, Desalination, 205 (2007), pp. 47–52

[26] K.-J. Hwang, C.-Y. Liao, K.-L. Tung, Effect of membrane pore size on the particle fouling in membrane filtration, Desalination, 234 (2008), pp. 16–23

[27] N. Ditzge, G. Soydemir, A. Karagunduz, B. Keskinler, Influence of type and pore size of membranes on cross flow microfiltration of biological suspension, J. Membr. Sci., 366 (2011), pp. 278–285

[28] M. Ousman, M. Bennasar, Determination of various hydraulic resistances during cross-flow filtration of a starch grain suspension through inorganic membranes, J. Membr. Sci., 105 (1995), pp. 1–21

[29] Z. Zhong, W. Li, W. Xing, N. Xu, Crossflow filtration of nanosized catalyst suspension using ceramic membranes, Sep. Purif. Technol., 76 (2011), pp. 223–230

[30] S. Hong, R.S. Faibish, M. Elimelech, Kinetics of permeate flux decline in crossflow membrane filtration of colloidal suspensions, J. Colloid Interface Sci., 196 (1997), pp. 267–277

[31] M.W. Chudacek, A.G. Fane, The dynamics of polarisation in unstirred and stirred ultrafiltration, J. Membr. Sci., 21 (1984), pp. 145–160

[32] M.J. Han, G.J.N.B. Barona, B. Jung, Effect of surface charge on hydrophilically modified poly(vinylidene fluoride) membrane for microfiltration, Desalination, 270 (2011), pp. 76–83

[33] W.-M. Lu, S.-C. Ju, Selective particle deposition in crossflow filtration, Sep. Sci. Technol., 24 (1989), pp. 517–540

[34] W.R. Bowen, X. Gosnaga, Properties of microfiltration membranes. Part 3. Effect of physicochemical conditions on crossflow microfiltration at alumina oxide membrane, IChemE Symp. Ser., 118 (1991), pp. 107–118

[35] K.J. Kim, A.G. Fane, M. Nystrom, A. Pihlajamaki, W.R. Bowen, H. Mukhtar, Evaluation of electroosmosis and streaming potential for measurement of electric charges of polymeric membranes, J. Membr. Sci., 116 (1996), pp. 149–159

[36] N. Xu, Y. Zhao, J. Zhong, J. Shi, Crossflow microfiltration of micro-sized mineral suspensions using ceramic membranes, Chem. Eng. Res. Des., 80 (2002), pp. 215–221

[37] Y. Zhao, Y. Zhang, W. Xing, N. Xu, Influences of pH and ionic strength on ceramic microfiltration of TiO2 suspensions, Desalination, 177 (2005), pp. 59–68
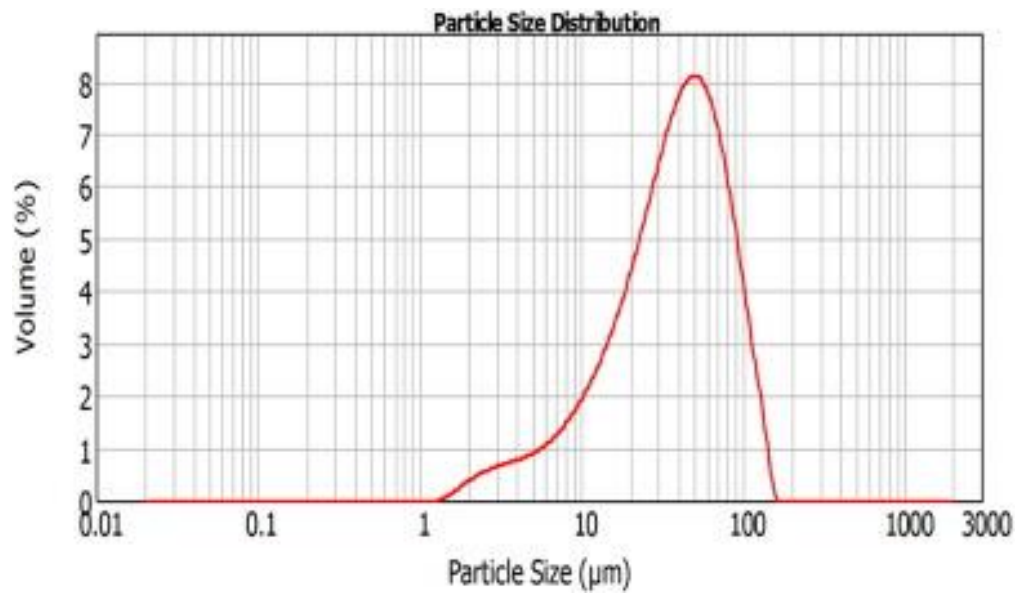
Fig. 1. Particle size distribution for the fractionized Amberlite IRA743 resin.
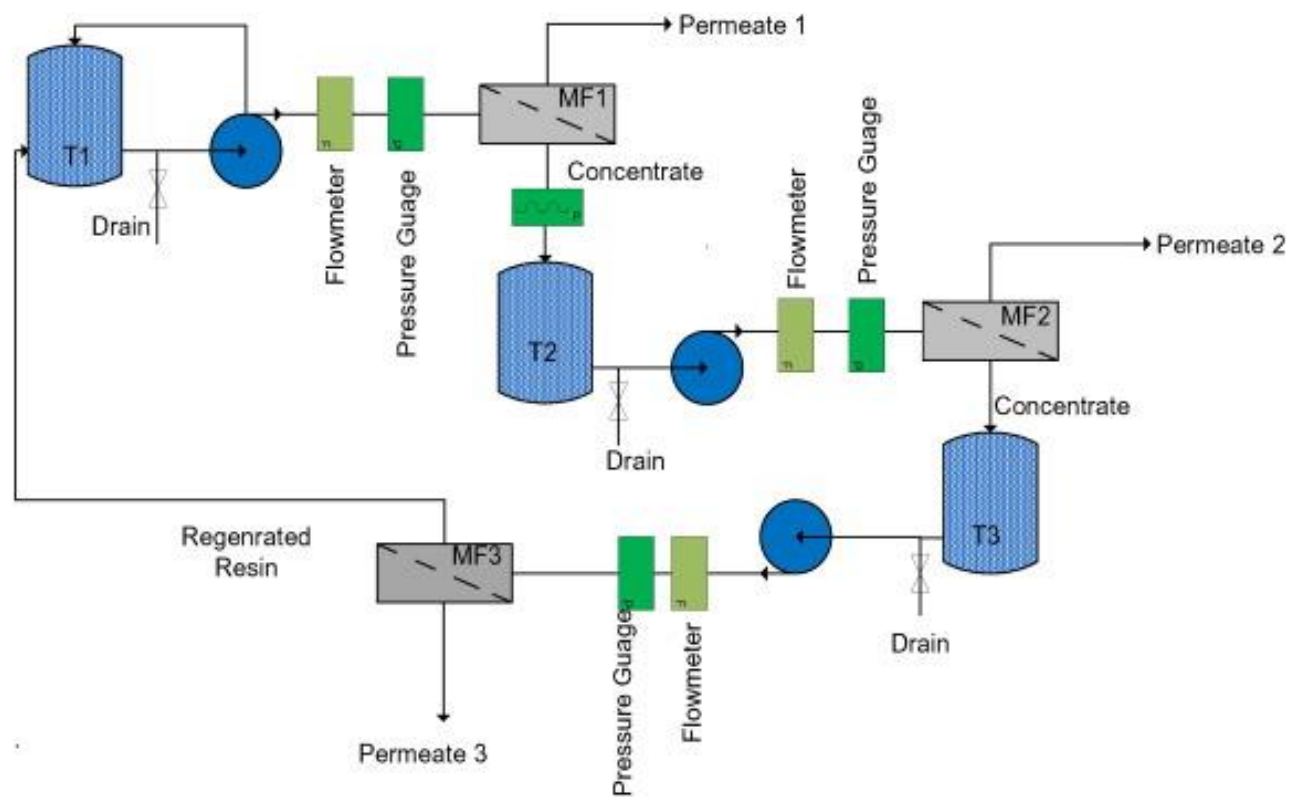
Fig. 2. A flow sheet of AMF system for boron removal from water used in the study.
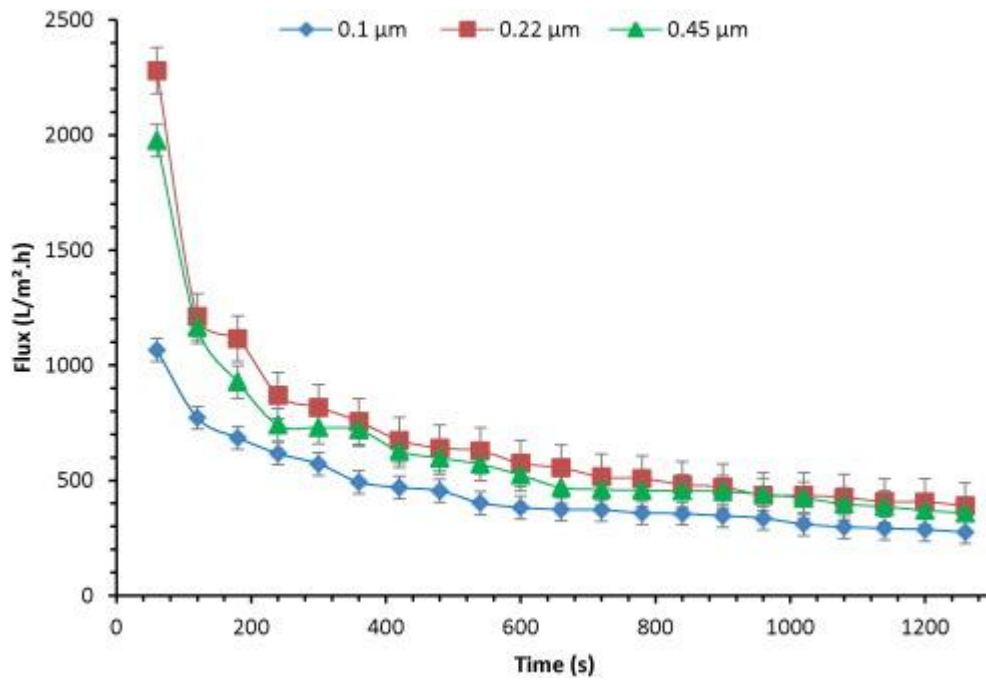
Fig. 3. Flux versus time during MF of the fractionized resin suspension with PVDF membranes of different pore size at operating pressure of 0.5 bar. The resin concentration is 1.0 g/L, pH = 6, and T = 25 °C.
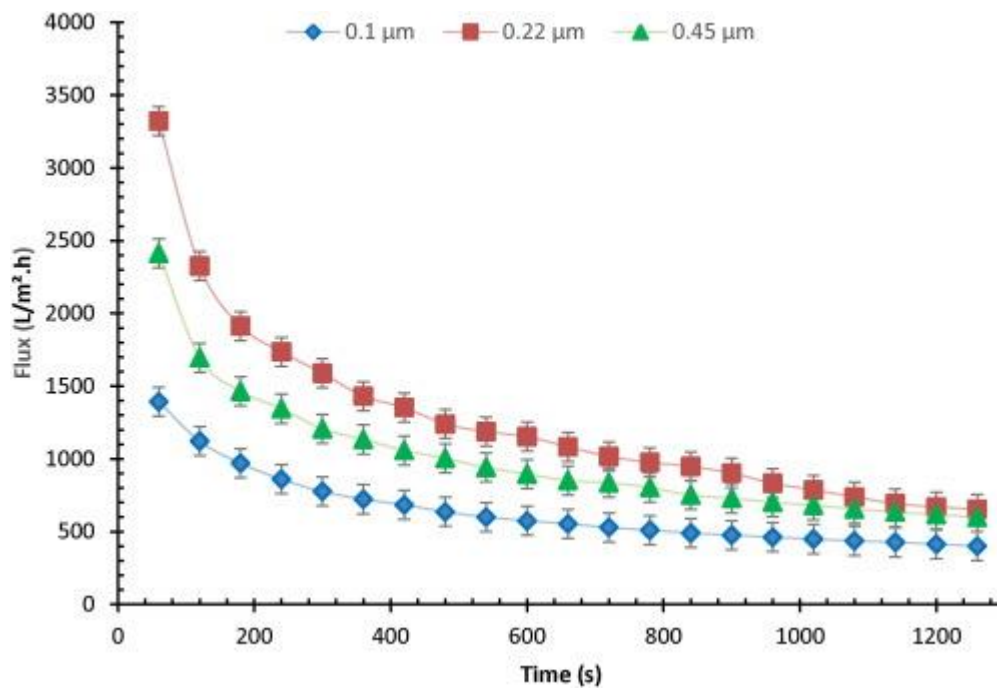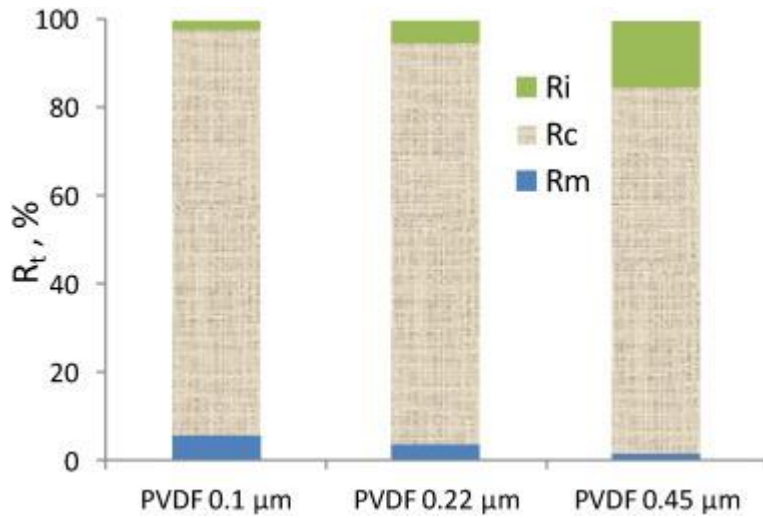

Fig. 4. Flux versus time during MF of the fractionized resin suspension with PVDF membranes of different pore size at operating pressure of 1.5 bar. The resin concentration is 1.0 g/L, pH = 6, and T = 25 °C.

Fig. 5. Experimental hydraulic resistances for PVDF membranes with different pore size during MF of the resin suspension. The resin concentration is 1.0 g/L, pH = 6, and T = 25 °C.
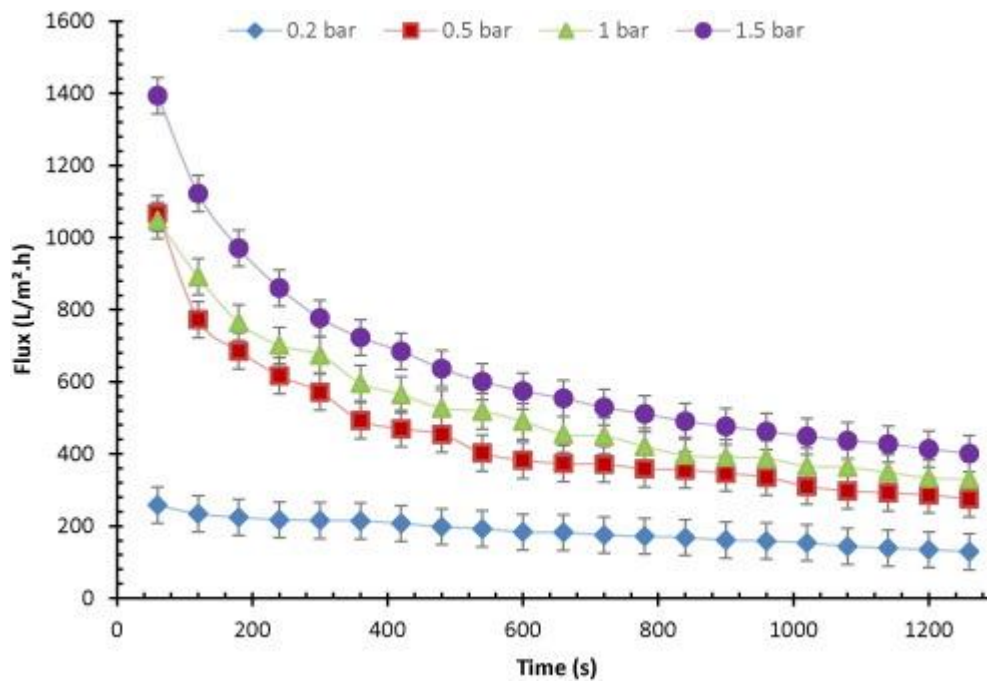
Fig. 6. Flux versus filtration time at different operating pressures during MF of the resin suspension with 0.1 μm PVDF membrane. The resin concentration is 1.0 g/L, pH = 6, and T = 25 °C.
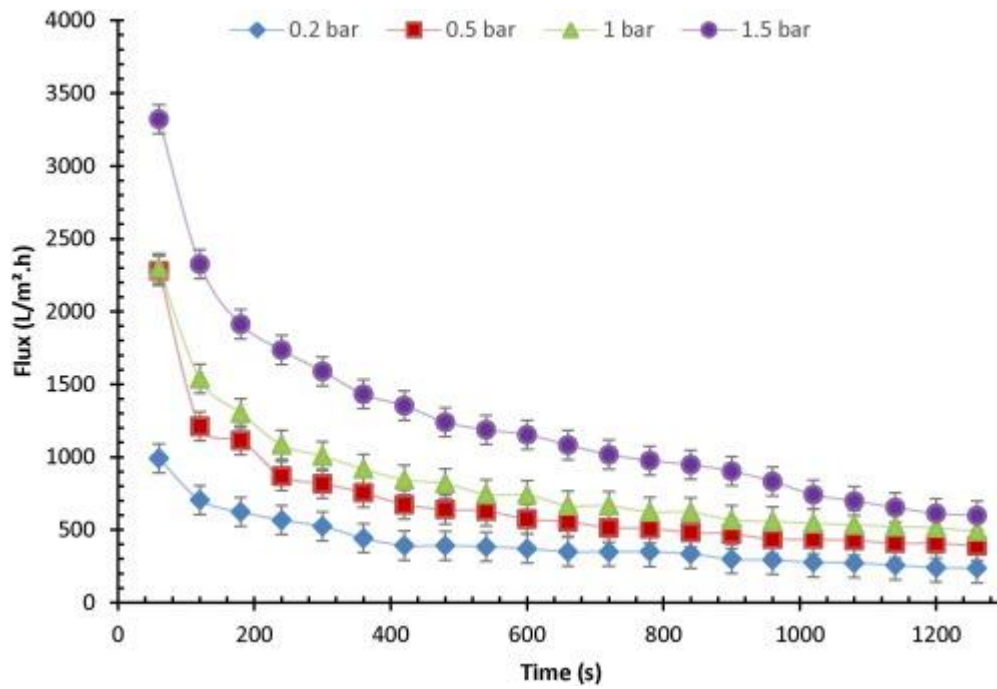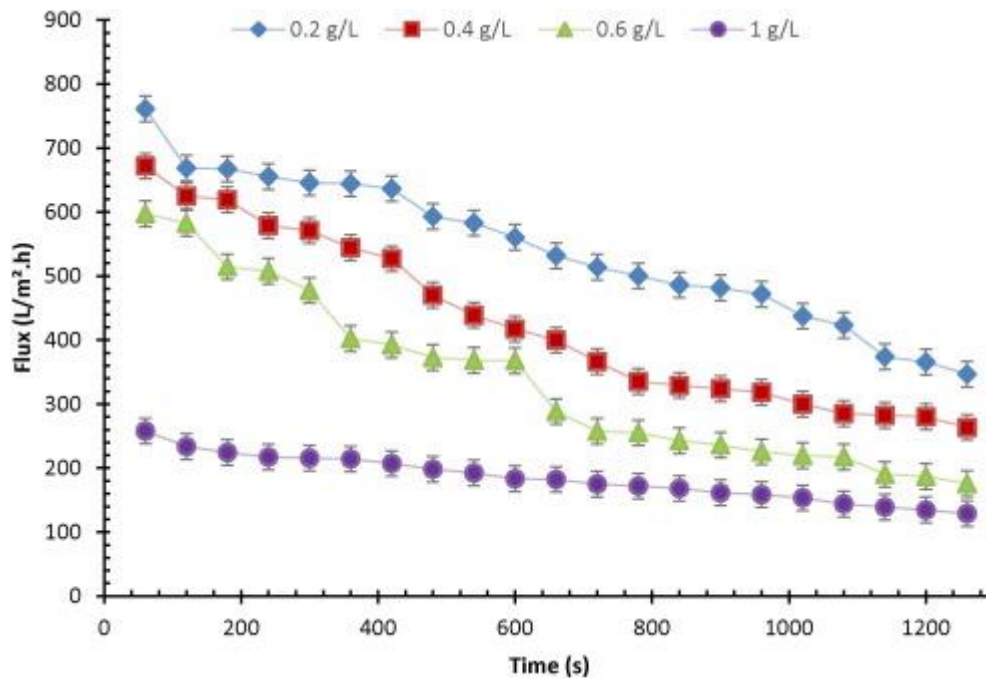
Fig. 7. Flux versus filtration time at different operating pressures during MF of the resin suspension with 0.22 μm PVDF membrane. The resin concentration is 1.0 g/L, pH = 6, and T = 25 °C.
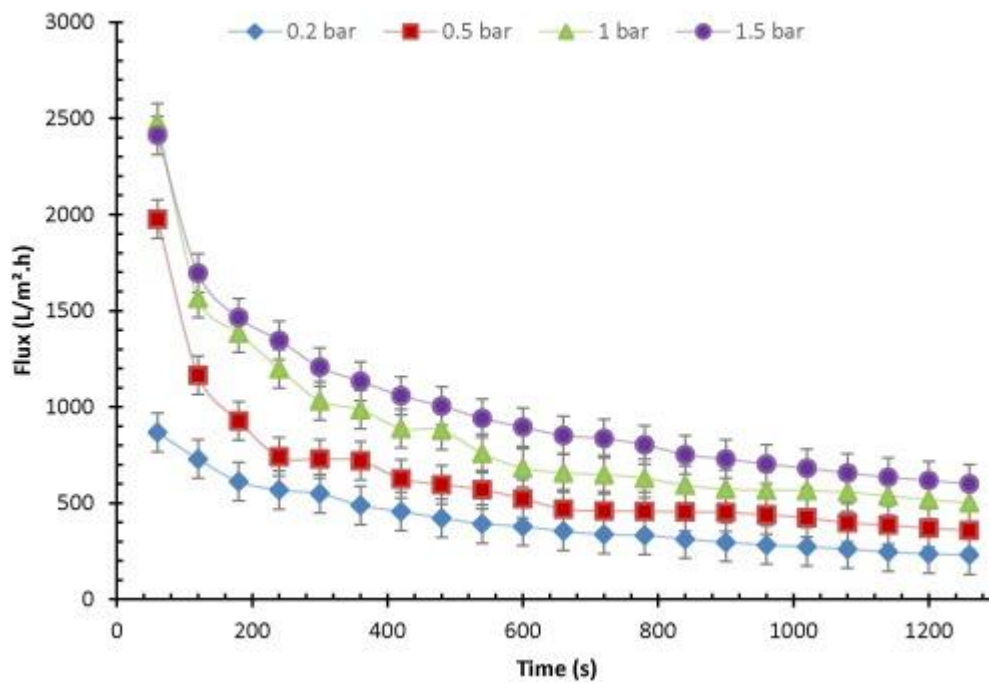
Fig. 8. Flux versus filtration time at different operating pressures during MF of the resin suspension with 0.45 μm PVDF membrane. The resin concentration is 1.0 g/L, pH = 6, and T = 25 °C.

Fig. 9. Flux versus filtration time during MF of fractionized resin suspensions of different concentrations with 0.1 μm PVDF membrane. Operating pressure is 0.2 bar, pH = 6, and T = 25 °C.
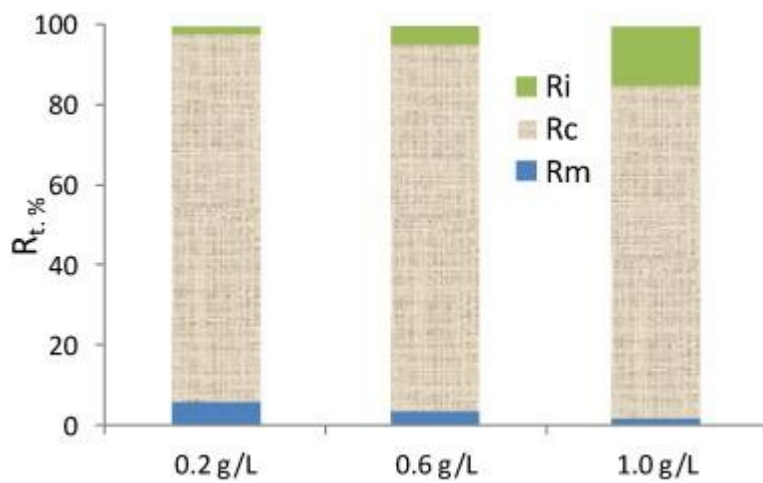
Fig. 10. Experimental hydraulic resistances for 0.1 μm PVDF membrane during MF of the resin suspensions of different concentrations. Operating pressure is 0.2 bar, pH = 6, and T = 25 °C.
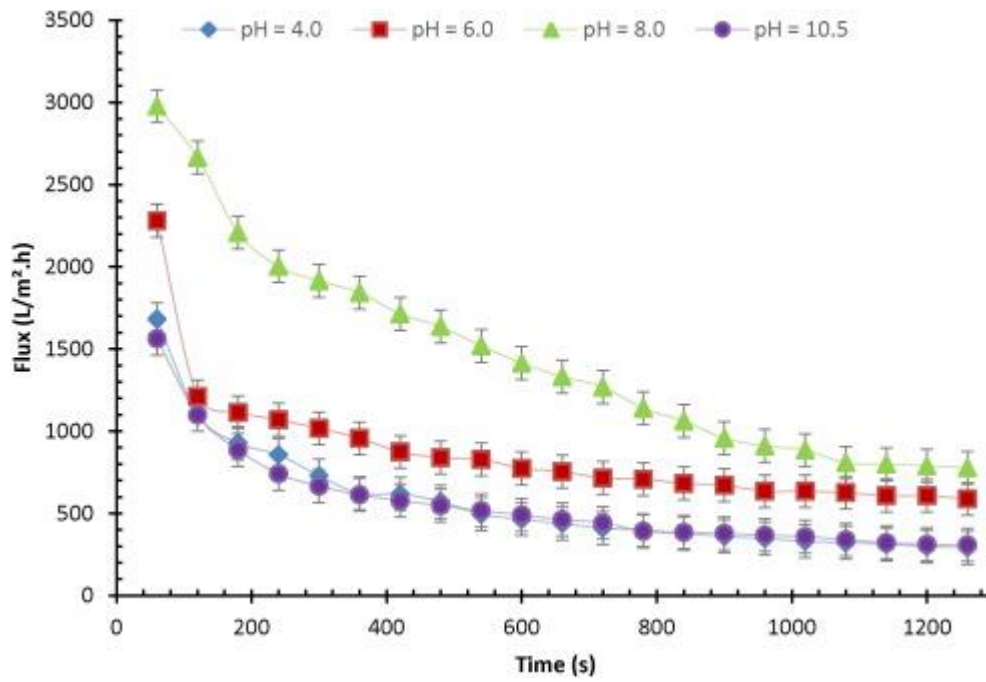
Fig. 11. Effect of pH on the membrane flux during MF of the fractionized resin suspension with 0.22 μm PVDF membrane. Operating pressure is 0.5 bar, resin concentration is 1 g/L, pH = 6, and T = 25 °C.
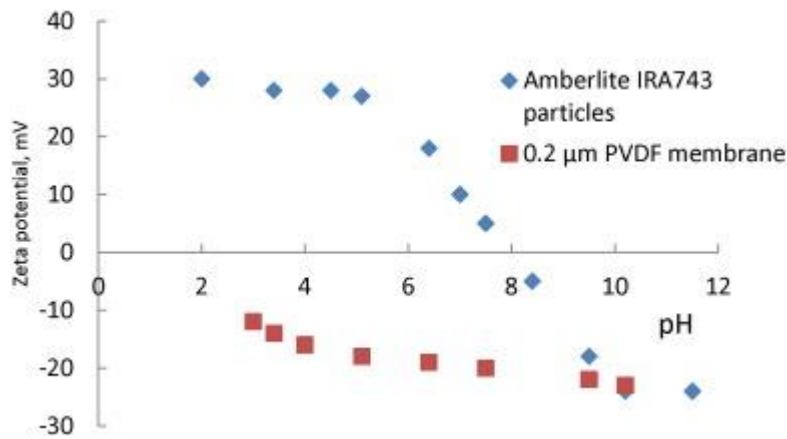

Fig. 12. Zeta potentials of Amberlite IRA743 resin particles and 0.22 μm PVDF membrane.
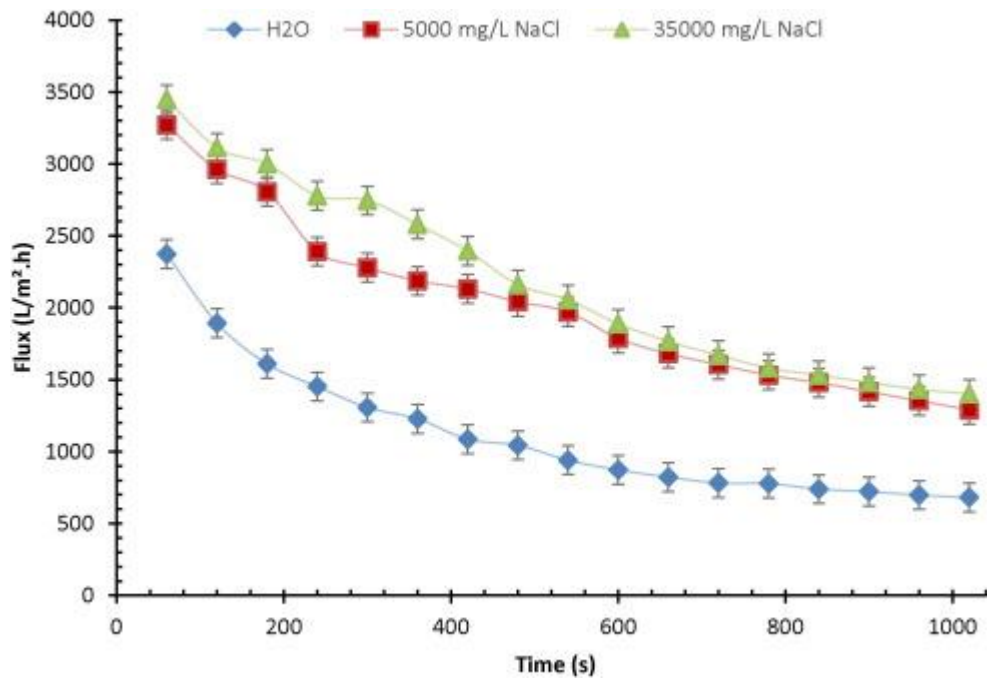
Fig. 13. Permeate flux for 0.22 μm PVDF membrane at different NaCl concentrations in the resin suspension. Operating pressure is 0.5 bar, resin dosage is 1 mg/L, pH = 6, T = 25 °C.
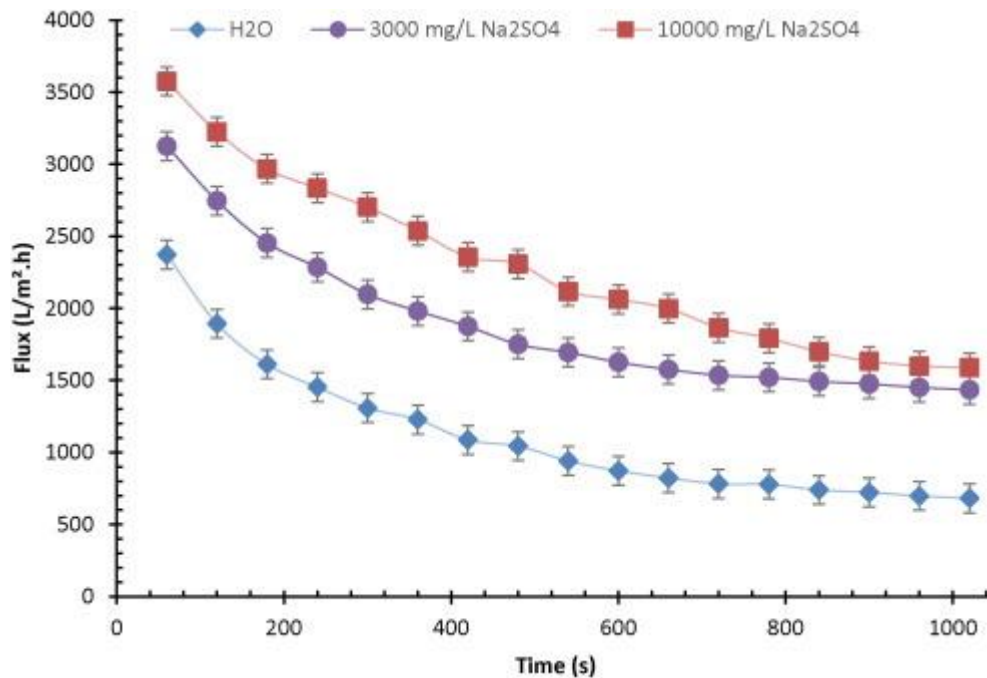

Fig. 14. Permeate flux for 0.22 μm PVDF membrane at different Na_2SO_4 concentrations in the feed suspension. Operating pressure is 0.5 bar, resin dosage is 1 mg/L. pH = 6, T = 25 °C.
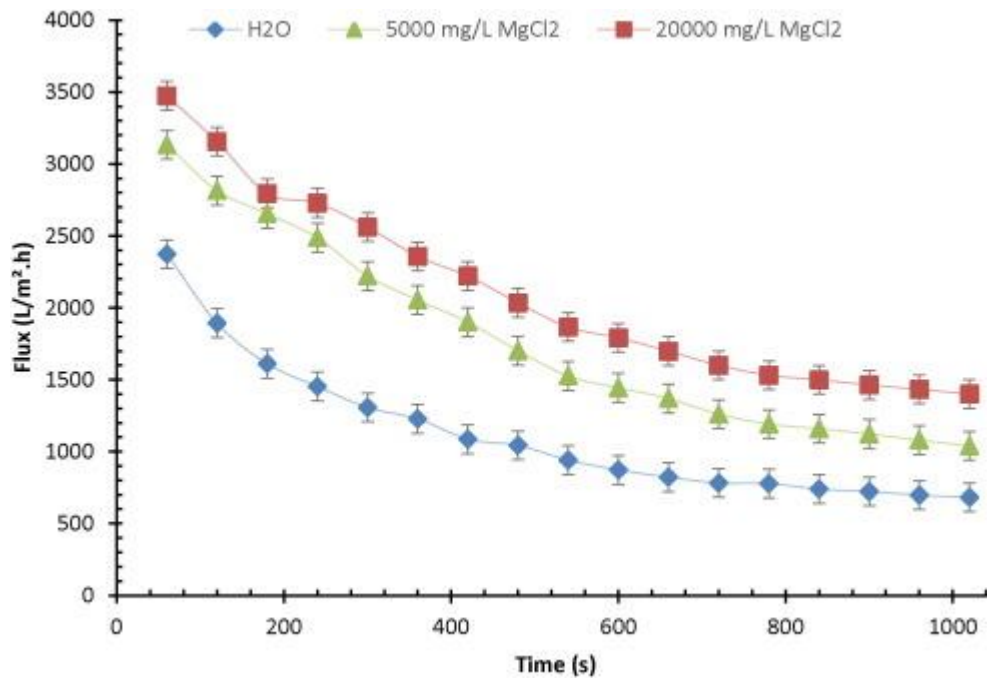
Fig. 15. Permeate flux for 0.22 μm PVDF membrane at different $MgCl_2$ concentrations in the feed suspension. Operating pressure is 0.5 bar, resin dosage is 1 mg/L. pH = 6, T = 25 °C.

Fig. 16. SEM images of the surface (a) and cross section (b) of neat 0.22 μm PVDF membranes and the membrane's surface (c) and the cross section (d) after concentrating of the boron-saturated resin suspension. The resin dosage = 1 g/L, pH = 6.
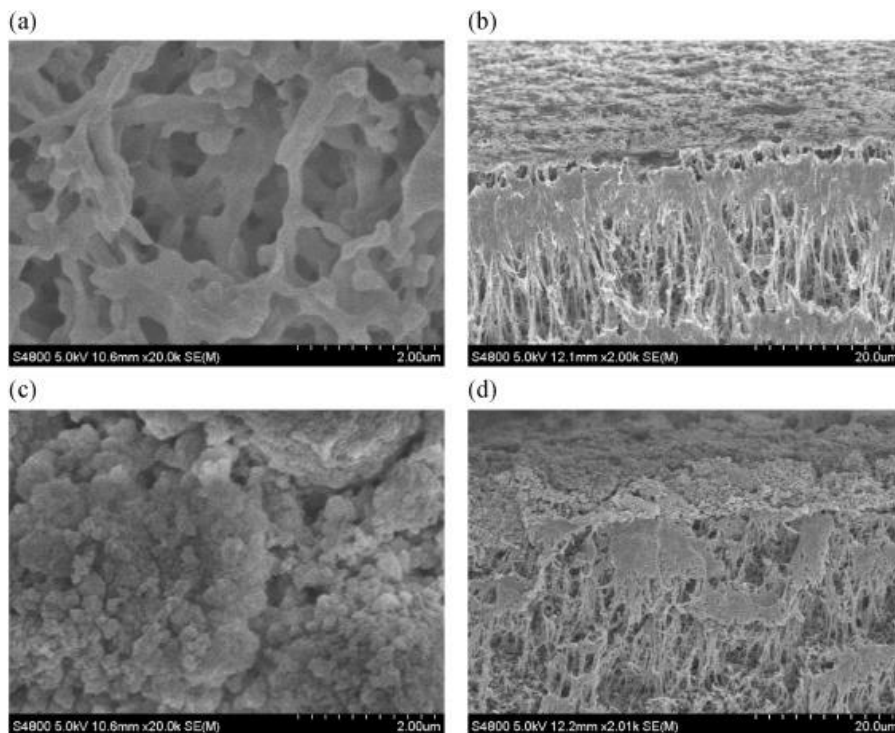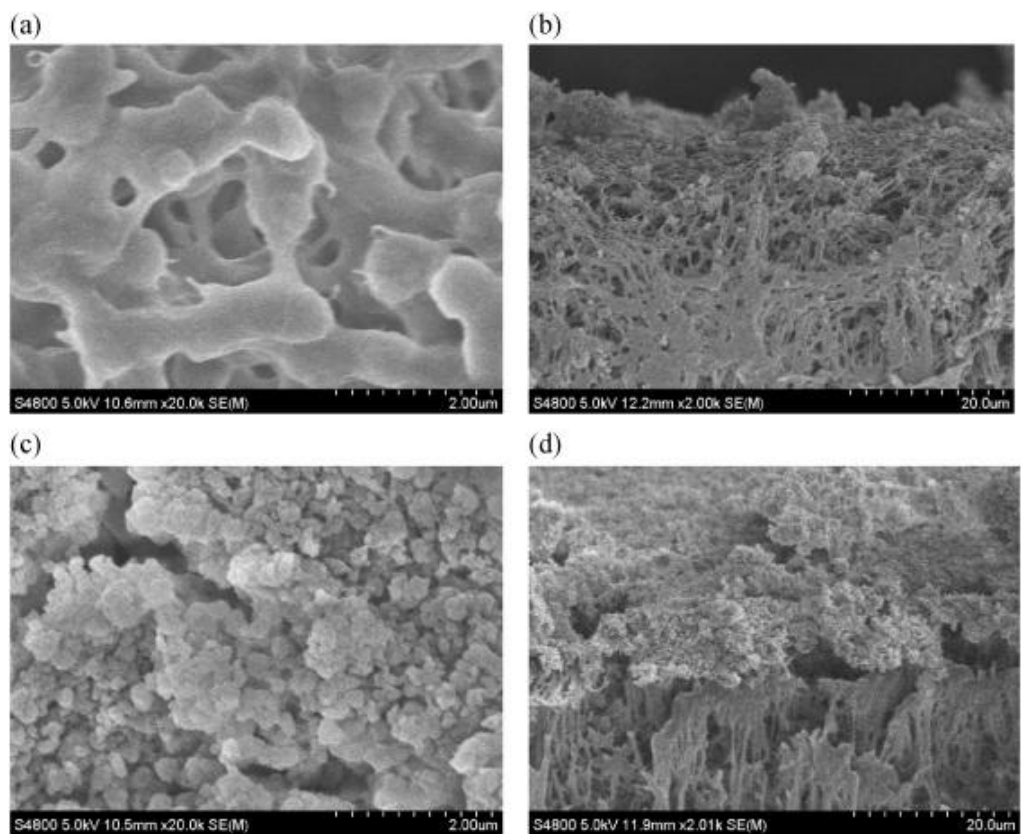
Fig. 17. SEM images of the surface (a) and cross section (b) of neat 0.45 μm PVDF membranes and the membrane's surface (c) and the cross section (d) after concentrating of the boron-saturated resin suspension. The resin dosage = 1 g/L, pH = 6.

List of Tables:

Table 1. Experimental hydraulic resistance (Rm, Ri and Rc) at different operating pressures during MF of the resin suspension with 0.1 µm PVDF membrane The resin concentration is 1.0 g/L, pH = 6, and T = 25 °C.

Hydraulic resistance 10^{11} m^{-1}	Operating pressure			
	0.2 bar	0.5 bar	1 bar	1.5 bar
Rm	0.2	0.2	0.1	0.1
Ri	0.1	0.3	0.8	1.5
Rc	4.2	9.5	21.1	36.8
Rt	4.5	10.0	22.0	38.4

Table 2. Experimental hydraulic membrane resistances (Rm, Ri and Rc) during MF of the resin suspension with 0.22 µm PVDF membrane at different MgCl$_2$ concentrations. The resin concentration is 1.0 g/L, pH = 6, and T = 25 °C.

Hydraulic resistance, 10^{11} m^{-1}	Feed		
	H$_2$O	5000 mg/L MgCl$_2$	20,000 mg/L MgCl$_2$
Rm	0.2	0.2	0.2
Ri	0.3	0.2	0.1
Rc	9.5	7.0	5.2
Rt	10.0	7.4	5.5

Table 3. Permeate flux with filtration time during MF separation of the resin suspension with 0.22 μm PVDF membrane after multiple boron sorption, elution and reconditioning steps. The ratio of the initial volume to the volume of the concentrated suspension is 5 and the resin dosage is 1 g/L for all the stages (the reloading of the fresh resin to keep the resin dosage as 1 g/L was used for the boron elution and reconditioning stages). Feed boron concentration is 5 mg/L, operating pressure is 0.5 bar and T = 25 °C.

Time, s	Flux, $L/m^2\,h$								
	Boron sorption stage			Boron elution stage			Reconditioning stage		
	Cycle 1	Cycle 2	Cycle 3	Cycle 1	Cycle 2	Cycle 3	Cycle 1	Cycle 2	Cycle 3
60	1929	1460	891	813	616	550	1806	876	617
120	1643	1267	872	686	605	545	1297	848	600
180	1460	1196	856	685	564	495	1125	766	579
240	1267	1124	837	621	524	474	968	703	571
300	1196	1021	799	558	496	441	876	674	556
360	1124	954	744	550	478	420	848	651	531
420	1091	901	701	508	444	400	766	617	524
480	1024	871	674	492	420	360	703	580	510
540	971	867	631	479	383	330	674	559	501
600	941	821	576	463	375	315	651	511	470
660	937	802	557	461	366	306	617	476	444
720	891	786	519	458	353	293	580	451	429
780	872	767	464	433	342	282	559	444	408
840	856	729	421	422	338	275			
900	837	674	400	418	330	264			
960	799	631	391						